



UNIVERSITY OF LEEDS

This is a repository copy of *A priori Nyström-method error bounds in approximate solutions of 1-D Fredholm integro-differential equations*.

White Rose Research Online URL for this paper:
<http://eprints.whiterose.ac.uk/135784/>

Version: Accepted Version

Article:

Fairbairn, AI and Kelmanson, MA (2019) A priori Nyström-method error bounds in approximate solutions of 1-D Fredholm integro-differential equations. *International Journal of Mechanical Sciences*, 150. pp. 755-766. ISSN 0020-7403

<https://doi.org/10.1016/j.ijmecsci.2018.09.021>

© 2018 Elsevier Ltd. Licensed under the Creative Commons Attribution-Non Commercial No Derivatives 4.0 International License (<https://creativecommons.org/licenses/by-nc-nd/4.0/>).

Reuse

This article is distributed under the terms of the Creative Commons Attribution-NonCommercial-NoDerivs (CC BY-NC-ND) licence. This licence only allows you to download this work and share it with others as long as you credit the authors, but you can't change the article in any way or use it commercially. More information and the full terms of the licence here: <https://creativecommons.org/licenses/>

Takedown

If you consider content in White Rose Research Online to be in breach of UK law, please notify us by emailing eprints@whiterose.ac.uk including the URL of the record and the reason for the withdrawal request.



eprints@whiterose.ac.uk
<https://eprints.whiterose.ac.uk/>

A priori Nyström-method error bounds in approximate solutions of 1-D Fredholm integro-differential equations

Abigail I Fairbairn and Mark A Kelmanson*

Department of Applied Mathematics, University of Leeds, Leeds LS2 9JT, UK

Abstract

A novel procedure is proposed for the *a priori* computation of error bounds for the ubiquitous Nyström solver applied to one-dimensional Fredholm integro-differential equations. The distinctive feature of the new approach is that the bounds are computed not only to spectral accuracy, but also explicitly, and in terms of only the numerical solution itself. Details are given of both the error analysis and its numerical implementation, and a corroborative asymptotic theory is developed in order to yield independent predictions of the convergence rates expected from Nyström discretisations of increasing order. All theory is first convincingly validated on a proof-of-concept continuous-kernel test problem whose solution is *a priori* known. The method is then applied to a novel integro-differential-equation formulation of a static, fourth-order, Euler-Bernoulli beam-deflection boundary-value problem in which the flexural rigidity varies along the beam, and for which no exact solution is attainable; in this case, validation of the resulting discontinuous-kernel approach is achieved using an asymptotic solution derived on the (realistic) assumption that variations in the cross-section of the beam occur on spatial scales an order of magnitude less than the beam's length and width. Potential limitations of the new approach are discussed.

Keywords: Integro-ordinary differential equations, error bounds, spectral collocation and related methods, numerical approximation of solutions

2010 MSC: 45J05, 65L70, 65M70, 74G15

1. Introduction

1.1. Motivation

A plethora of literature is devoted to the computation of approximate solutions of engineering problems using integral-equation techniques, which offer advantages over differential solvers on several fronts. Specifically, the principal advantages of reformulating a two-point boundary-value problem (BVP) as an equivalent Fredholm integral equation (FIE) are: (i) the latter can often be solved to spectral accuracy using collocation employing quadrature abscissae at the roots or extrema of orthogonal polynomials; (ii) the boundary conditions (BCs) can be incorporated either exactly or to spectral accuracy [24, 8] rather

*Corresponding author email address: M.Kelmanson@leeds.ac.uk

than by, e.g., one-sided finite-difference formulae of low-order accuracy, and (iii) discretisation of higher-order derivatives in the original BVP using higher powers of ill-conditioned [6] differentiation matrices is avoided.

Although approximation methods for the solution of FIEs have burgeoned since the 1960s, only a handful have examined the aspect, of obvious practical importance, of *a priori* error estimates. Moreover, even in these few studies, convergence to zero (with an increasing number of collocation nodes) of errors is either merely demonstrated by comparison against known solutions of test problems, or the order of convergence, rather than quantification of the error itself, is estimated. An overview of, and a method to circumvent this shortcoming is given in [12], in which the present authors disseminate the first (to our knowledge) analysis for and implementation of a technique for the explicit computation and quantification of spectrally accurate error bounds using *only the approximate, computed numerical solution* of the FIE. Though test problems are indeed considered in [12], it is stressed that these are used only to demonstrate that the new *a priori* theoretically predicted error estimates agree to spectral accuracy with the *a posteriori* calculated ones. That is, in the usual practical situation that the exact solution is unknown, the new approach offers a cheap and efficient means of computing spectrally accurate *a priori* error tolerances.

In this paper an approach is developed for predicting spectrally accurate error bounds in the approximate solution of BVPs reformulated as integro-differential equations (IDEs); note that the present work does not use the term integro-differential to signify spatial integration coupled with temporal differentiation¹; here, both differential and integral operators are spatial. Accordingly, the aim of the present work is to analyse and to develop a novel error-prediction theory, and to implement it by embedding it into a Nyström-based procedure for approximating the solution of IDEs. In the last two decades, IDEs have frequently arisen in the study of engineering problems [9, 10, 20, 17, 21, 26], in the last of which a statement is made that partially motivates the need for the present work: “... *numerical methods are usually applied in the literature to deal with the resulting integro-differential equations*² ... *which are shown to be time consuming and the numerical errors are sometimes hard to detect for some specific nonlocal kernels.*” In keeping with this motivation, a novel formulation and spectrally accurate solution of an Euler-Bernoulli beam-deflection problem is subsequently presented.

1.2. Background, aims and objectives

Further discussion is facilitated by considering a canonical form of IDE relative to which prior art and present goals can be clarified. As stated above, there is a considerable literature devoted to the computation of the approximate solution of IDEs, for the unknown function $u(x)$, whose normalised canonical form [1,

¹ For example, as in the peridynamic theory of solids (see, e.g., [23, 11]).

² Governing the static bending of Euler-Bernoulli beams.

eqns (18) and (24)] on the interval $[-1, 1]$ is

$$u(x) - \mu(x) u'(x) - \lambda \int_{-1}^1 K(x, \tilde{x}) u(\tilde{x}) d\tilde{x} = f(x), \quad x \in [-1, 1], \quad (1)$$

in which the source function $f : [-1, 1] \rightarrow \mathbb{R}$, the kernel $K : [-1, 1] \times [-1, 1] \rightarrow \mathbb{R}$ and coefficient function $\mu : [-1, 1] \rightarrow \mathbb{R}$ are prescribed functions of $x, \tilde{x} \in [-1, 1]$, and $\lambda \in \mathbb{R}$ is a constant. For now, discussion of the BC that augments (1) is deferred until §2. The Fredholm IDE (1) is of practical relevance: for example, the fourth-order Euler-Bernoulli ordinary differential equation for the small deflection $u(x)$ of a simply-supported loaded beam of non-constant cross-section (and hence flexural rigidity) may be reformulated as an IDE by repeated integration to yield an IDE of precisely the form (1); full details of a novel derivation of this reformulation, and a generic extension thereof, are provided in Appendix B.

Many authors [18, 4, 27, 15, 16, 7, 28, 5, 3, 19, 22] have developed a diverse range of numerical methods for obtaining the solution of not only (1) but also its extension to higher differential orders. The primary aim of the present paper is to develop and to implement a computational method that yields explicitly computable and spectrally accurate *a priori* error predictions for the numerical solution of (1) using Nyström-type methods. Indeed, in spite of the considerable amount of apparently related literature, the formal development of a mathematical framework for conducting error analyses continues to be relatively rare. For example, despite the diversity of the numerical approaches deployed in the above-cited literature, only a few of the citations contain even brief discussion of errors, and none presents *a priori* computable error estimates, let alone to the spectral accuracy obtained herein. [18, §2] proves convergence to zero of the Nyström errors in the Fredholm component resulting from an IDE-to-IE conversion; [15, §3] computes an error function as a solution of a perturbation IDE that itself is subject to discretisation error; [28, §4] discusses the accuracy of the solution in terms of an estimated error function, though this is not used to make quantifiable error-bound predictions *per se*; [19, §4] includes a brief error analysis of a wavelet approach, giving error bounds for only the first derivative of the solution rather than the solution itself, and; [2, §4] proves a convergence theorem for the iterative method, but does not explicitly analyse errors. By contrast, the authors' recent companion paper [13] extends the IDE-to-FIE approach of [18] to obtain the first-ever spectrally accurate *a priori* error estimates of numerical solutions of (1).

Accordingly, it is hoped that the present work will augment the existing literature in a novel and useful way by providing a method for computing error bounds for the (Nyström) numerical solution of (1) not only *a priori*, but also, as in [13], explicitly in terms of *only the numerical solution itself*. As it transpires, the predicted bounds are spectrally accurate for a diverse class of problems, adding to the merit of the approach. Additionally, the method presented in this paper can be extended to admit higher-order derivatives of $u(x)$ in (1) whereas the transformation method presented in [18, 13] is restricted to first-order IDEs.

The remainder of this paper is structured as follows. In §2 is presented the IDE problem and its Nyström discretisation on nodal distributions based on Gauss-Legendre, -Radau and -Lobatto formulae. For clarity, technical details of the implementation of two distinct procedures for (direct and indirect) incorporation

of the BC that augments (1) are deferred to Appendix A. The main error analysis of §3 is split into two parts: the fundamental operator theory in §3.1 that underpins all results required for both implementing the method and conducting the error-bound computation, and; an asymptotic approach is developed in §3.2 to yield *a priori* predictions of the convergence rates of the computed errors. Presented in §4 is a convincing validation of all theory via implementation on two disparate test problems: in §4.1, a proof-of-concept problem with *a priori* known solution and, in §4.2 a practical Euler-Bernoulli beam-deflection problem (newly formulated in Appendix B) for which an exact solution is unattainable due to the spatially varying flexural rigidity of the beam, and for which the error-bound prediction is therefore of genuine practical importance. The paper culminates in §4.3 with a general discussion of both the findings of the present work and the limitations of the theory presented.

2. Problem outline and spectral discretisation

First, IDE (1) is augmented by the boundary condition (hereafter BC)

$$u(\xi) = \zeta, \quad \xi \in [-1, 1], \quad (2)$$

in which $\zeta \in \mathbb{R}$ is a prescribed constant. Note that (2) is not intended to convey that u is constant throughout $[-1, 1]$, but rather that the BC can be enforced at any location ξ in $[-1, 1]$. In symbolic form, (1) is

$$u - \mu \mathcal{D} u - \lambda \mathcal{K} u = f \quad (3)$$

in which $u, f \in \mathcal{C} \equiv C[-1, 1]$, the Banach space with supremum norm $\|\cdot\|$ on which the action of differential operator \mathcal{D} on u is defined by

$$\mathcal{D} u = (\mathcal{D} u)(x) \equiv u'(x), \quad (4)$$

where a prime denotes differentiation with respect to x . The action of the compact integral operator \mathcal{K} on u in (3) is defined by

$$\mathcal{K} u = (\mathcal{K} u)(x) \equiv \int_{-1}^1 K(x, \tilde{x}) u(\tilde{x}) d\tilde{x}. \quad (5)$$

For later use, it is convenient to define the linear operator \mathcal{A} by

$$\mathcal{A} \equiv \mu \mathcal{D} + \lambda \mathcal{K}. \quad (6)$$

The present error analysis utilises approximate solutions of (1) and (2) in which the actions of \mathcal{D} and \mathcal{K} have been approximated to spectral accuracy using finite-rank operators \mathcal{D}_N and \mathcal{K}_N for, respectively, discrete differentiation and numerical quadrature. Accordingly, procedures for implementing \mathcal{D}_N and \mathcal{K}_N are now established.

It is well known that optimal N -node distributions for constructing the differentiation matrix representing \mathcal{D}_N are based on the roots of Chebyshev polynomials [24]. However, when the weight function is

unity in the integrand in (5), optimal nodes for the quadrature rule representing \mathcal{K}_N are given by roots of Legendre polynomials. The method presently developed therefore employs a Legendre-root distribution to construct a near-optimal \mathcal{D}_N and an optimal \mathcal{K}_N ; the effects of this trade-off in optimality is performed in order to preclude computationally expensive interpolation between the two node sets. In the hybrid integro-differential approximation procedure now developed, the action of \mathcal{K}_N is given by

$$\mathcal{K} u \approx \mathcal{K}_N u \equiv \sum_{j=1}^N w_{j,N}^{(\nu)} K(x, \tilde{x}_{j,N}^{(\nu)}) u(\tilde{x}_{j,N}^{(\nu)}), \quad (7)$$

wherein $w_{j,N}^{(\nu)}$ and $\tilde{x}_{j,N}^{(\nu)}$ are respectively the weights and abscissae of the N -node quadrature rule incorporating ν pre-specified nodes and the abscissae are ordered with $1 \leq i < j \leq N \Rightarrow -1 \leq \tilde{x}_{i,N} < \tilde{x}_{j,N} \leq 1$. Specifically [12], $\nu = 0, 1$ and 2 correspond to, in decreasing order of optimality, Gauss-Legendre, Legendre-Gauss-Radau and Legendre-Gauss-Lobatto nodes respectively. Much of the ensuing analysis is thus dependent upon ν which, for the sake of clarity, is henceforth notationally suppressed unless it quantitatively affects a result. It will also be assumed that integer suffices i and j in all subsequent discrete formulae satisfy $1 \leq i, j \leq N$.

On all node sets, the action of \mathcal{D}_N is given by

$$\mathcal{D} u \approx \mathcal{D}_N u = \sum_{j=1}^N L'_{j,N}(x) u(\tilde{x}_{j,N}), \quad (8)$$

wherein the first derivative of the standard Lagrange basis function $L_{j,N}(x)$ is given by

$$L'_{j,N}(x) = \frac{(x - \tilde{x}_{j,N}) p'_N(x) - p_N(x)}{(x - \tilde{x}_{j,N})^2 p'_N(\tilde{x}_{j,N})}, \quad (9)$$

in which $p_N(x)$ is the monic polynomial

$$p_N(x) \equiv \prod_{j=1}^N (x - \tilde{x}_{j,N}), \quad (10)$$

whose (ν -dependent) roots are the abscissae $\tilde{x}_{j,N}$ defined in (7). Note that, if $u'(x)$ in (1) is replaced by $u^{(m)}(x)$, then \mathcal{D} in (6) is replaced by \mathcal{D}^m and (8) is replaced by

$$\mathcal{D}^m u \approx \mathcal{D}_N^{(m)} u = \sum_{j=1}^N L_{j,N}^{(m)}(x) u(\tilde{x}_{j,N}), \quad (11)$$

and recall that the authors' related method [13] can be applied only when $m = 1$. Using (7) and (8), the approximate solution $u_N(x)$ of (1) satisfies the discretised equation

$$u_N(x) - \mu(x) \sum_{j=1}^N L'_{j,N}(x) u_N(\tilde{x}_{j,N}) - \lambda \sum_{j=1}^N w_{j,N} K(x, \tilde{x}_{j,N}) u_N(\tilde{x}_{j,N}) = f(x), \quad (12)$$

whose symbolic form is (*cf.* (3))

$$u_N - \mu \mathcal{D}_N u_N - \lambda \mathcal{K}_N u_N = f, \quad (13)$$

suggesting (cf. (6)) that the linear operator \mathcal{A}_N that approximates \mathcal{A} is defined by

$$\mathcal{A}_N \equiv \mu \mathcal{D}_N + \lambda \mathcal{K}_N . \quad (14)$$

Defining $\alpha_{j,N}(x)$ by

$$\alpha_{j,N}(x) \equiv \mu(x) L'_{j,N}(x) + \lambda w_{j,N} K(x, \tilde{x}_{j,N}) , \quad (15)$$

discretisation of (12) yields

$$u_N(x) - \sum_{j=1}^N \alpha_{j,N}(x) u_N(\tilde{x}_{j,N}) = f(x) , \quad (16)$$

so that, by (14)–(16),

$$\mathcal{A}_N u_N(x) \equiv \sum_{j=1}^N \alpha_{j,N}(x) u_N(\tilde{x}_{j,N}) . \quad (17)$$

Collocating (16) at nodes $x = \tilde{x}_{i,N}$ yields the $N \times N$ linear system

$$\sum_{j=1}^N (\delta_{ij} - \alpha_{j,N}(\tilde{x}_{i,N})) u_N(\tilde{x}_{j,N}) = f(\tilde{x}_{i,N}) , \quad i = 1(1)N . \quad (18)$$

In matrix form, (18) is

$$(\mathbf{I}_N - \mathbf{A}_N) \mathbf{u}_N = \mathbf{f}_N , \quad (19)$$

in which matrix and vector entries are given by

$$\{\mathbf{I}_N\}_{i,j} = \delta_{ij} , \quad \{\mathbf{A}_N\}_{i,j} = \alpha_{j,N}(\tilde{x}_{i,N}) , \quad \{\mathbf{u}_N\}_i = u_N(\tilde{x}_{i,N}) \quad \text{and} \quad \{\mathbf{f}_N\}_i = f(\tilde{x}_{i,N}) . \quad (20)$$

Note that the matrix \mathbf{A}_N is the linear combination

$$\mathbf{A}_N = \text{diag}\{\mu(\tilde{x}_{i,N})\} \mathbf{D}_N + \lambda \mathbf{K}_N \quad (21)$$

of the differentiation and quadrature matrices \mathbf{D}_N and \mathbf{K}_N respectively given by

$$\{\mathbf{D}_N\}_{i,j} = L'_{j,N}(\tilde{x}_{i,N}) \quad \text{and} \quad \{\mathbf{K}_N\}_{i,j} = w_{j,N} K(\tilde{x}_{i,N}, \tilde{x}_{j,N}) . \quad (22)$$

The discrete formulation is completed by incorporating the BC (2), thereby reducing (18) to an $(N - 1) \times (N - 1)$ system: this can be done in one of two ways, depending on whether or not ξ in (2) coincides with a quadrature node $\tilde{x}_{j,N}$. In what follows, \tilde{u}_N and \hat{u}_N will denote numerical solutions obtained via, respectively, so-called direct (“case-1”) and indirect (“case-2”) BC enforcement. Since the present main focus is on the novel error analysis, details concerning the implementation of the two different cases are deferred to Appendix A.

3. Error Analysis

The theoretical framework for the error analysis of the IDE Nyström method in §2 is now presented, the goal being the determination of *a priori* accurate bounds for the error norms $\|u - \tilde{u}_N\|$ and $\|u - \hat{u}_N\|$

wherein, as stated above, the supremum norm of the Banach space $\mathcal{C} = C[-1, 1]$ is implied. This analysis extends the pure-IE approach in [12] in order to circumvent the presence of the unbounded differential operator \mathcal{D} , which precludes the standard approach that implicitly utilises $\|\mathcal{D}\|$, whose unboundedness violates the conditions underlying the theorem [4, Thm. 4.1.2] on which the pure-IE error analysis is founded. A formal operator approach for circumventing this issue is now derived.

3.1. Operator theory

Throughout this section, the action of all (linear, either single or compound) operators \mathcal{P} on functions $g(x)$ for $x \in [-1, 1]$ is to be interpreted as $\mathcal{P}g(x) \equiv (\mathcal{P}g)(x)$. Using this notation, the operator form of (1) is, from (3) and (6),

$$u(x) - \mathcal{A}u(x) = f(x), \quad (23)$$

$$u(\xi) = \zeta. \quad (24)$$

The corresponding operator form of the Nyström implementation of (12) is established by noting that tildes and hats can be respectively dropped from (A.5) and (A.11) to yield the generic interpolation formula

$$u_N(x) = f(x) + \alpha_{k,N}(x) u_N^*(\tilde{x}_{k,N}) + \sum_{\substack{j=1 \\ j \neq k}}^N \alpha_{j,N}(x) u_N^*(\tilde{x}_{j,N}), \quad x \in [-1, 1], \quad (25)$$

which both includes the BC (A.2) or pseudo-BC (A.8), and may be written using (A.1) as

$$u_N(x) = f(x) + \mathcal{A}_N u_N^*(x), \quad x \in [-1, 1]. \quad (26)$$

Note that, as stated in Appendix A, the notation $u_N^*(\tilde{x}_{j,N})$ in (25) and (26) indicates a nodal value of $u_N(x)$ determined by collocation in the first stage of the Nyström process, rather than by interpolation in the second stage. Subtracting $\mathcal{A}_N u_N(x)$ from both sides of (26), definitions (17) and (A.1) yield

$$\begin{aligned} u_N(x) - \mathcal{A}_N u_N(x) &= f(x) + \mathcal{A}_N (u_N^*(x) - u_N(x)) \\ &= f(x) + \sum_{j=1}^N \alpha_{j,N}(x) (u_N^*(\tilde{x}_{j,N}) - u_N(\tilde{x}_{j,N})), \quad x \in [-1, 1], \end{aligned} \quad (27)$$

in which all terms in the sum vanish except for the one with $j = k$ because this is the only index for which, by (A.6) and (A.13), the collocated nodal value $u_N^*(\tilde{x}_{j,N})$ is not equal to the interpolated value $u_N(\tilde{x}_{j,N})$. Therefore, defining the *residual* by

$$\rho_N(x) = \alpha_{k,N}(x) (u_N(\tilde{x}_{k,N}) - u_N^*(\tilde{x}_{k,N})), \quad x \in [-1, 1], \quad (28)$$

the required operator form of (12) that incorporates the BC $u_N^*(\tilde{x}_{k,N}) \leftarrow \widehat{\zeta}$ or $u_N^*(\tilde{x}_{k,N}) \leftarrow \widetilde{\zeta}$ is

$$u_N(x) - \mathcal{A}_N u_N(x) = f(x) - \rho_N(x). \quad (29)$$

It is noteworthy that, unless $\alpha_{k,N}(x) \equiv 0$, the residual does not vanish; by (A.6) in case 1 (the direct BC (A.2)) and by (A.13) in case 2 (the indirect BC (A.8)). However, as discussed above, $\alpha_{k,N}(x)$ will vanish with zero probability for the arbitrary values listed immediately after (A.8).

Note that, in the absence of (24), the unbounded differentiation operator \mathcal{D} in \mathcal{A} admits two different solutions³ $u \neq v$ of (23) for which $(\mathcal{J} - \mathcal{A})u = f$ and $(\mathcal{J} - \mathcal{A})v = f$, where \mathcal{J} is the identity operator; that is, unlike its counterpart $\mathcal{J} - \lambda\mathcal{K}$ in the pure FIE, $\mathcal{J} - \mathcal{A}$ is not one-to-one and hence not invertible, so that the theory of compact operators underlying the standard FIE error analysis [4, Thm. 1.1] cannot be applied.

The problem can be reformulated in terms of bounded operators by first defining the *punctured* identity operator $\bar{\mathcal{J}}$ whose action on the function $v \in \mathcal{C}$ is defined by

$$\bar{\mathcal{J}}v(x) \equiv \bar{v}(x) = \begin{cases} v(x) & x \neq \xi \\ 0 & x = \xi \end{cases}; \quad (30)$$

that is, $v(x)$ is punctured at the value of x at which the BC is assigned. Operating on both sides of the exact IDE (23) with $\bar{\mathcal{J}}$ yields $\bar{\mathcal{J}}(\mathcal{J} - \mathcal{A})u(x) = \bar{\mathcal{J}}f(x)$, or, equivalently, by defining $\bar{\mathcal{A}} = \bar{\mathcal{J}}\mathcal{A}$ and using (30),

$$(\bar{\mathcal{J}} - \bar{\mathcal{A}})u(x) = \bar{f}(x). \quad (31)$$

Operating on both sides of (29) with $\bar{\mathcal{J}}$ and defining $\bar{\mathcal{A}}_N \equiv \bar{\mathcal{J}}\mathcal{A}_N$, there results

$$(\bar{\mathcal{J}} - \bar{\mathcal{A}}_N)u_N(x) = \bar{f}(x) - \bar{\rho}_N(x). \quad (32)$$

Subtraction of (32) from (31), addition of $\bar{\mathcal{A}}u_N(x)$ to both sides and factorisation of $u(x) - u_N(x)$ yields an operator equation for the error in the form

$$(\bar{\mathcal{J}} - \bar{\mathcal{A}})(u(x) - u_N(x)) = (\bar{\mathcal{A}} - \bar{\mathcal{A}}_N)u_N(x) + \bar{\rho}_N(x), \quad (33)$$

which reveals that the error in the numerical solution $u_N(x)$ is a combination of (i) the residual associated with the imposition of a pseudo-BC at the first stage of the Nyström process, and (ii) the truncation error due to the discretisation of both the differential and integral operators in the original IDE.

By inclusion of BC (24), equation (33) has a unique solution and thus $\bar{\mathcal{J}} - \bar{\mathcal{A}}$ is one-to-one and invertible; recall that $\mathcal{J} - \mathcal{A}$ was not⁴. Suppressing the uniform argument x throughout, inversion of (33) yields

$$u - u_N = (\bar{\mathcal{J}} - \bar{\mathcal{A}})^{-1} \bar{\mathcal{J}} \{ (\mathcal{A} - \mathcal{A}_N)u_N + \rho_N \}, \quad (34)$$

³For example, in the case of a separable kernel, a “free” IDE reduces to a first-order ODE whose solution, determined via an integrating factor, includes an arbitrary constant.

⁴A well-known discrete manifestation of this is the non-invertibility of \mathbf{D}_N and invertibility of $\bar{\mathbf{D}}_N$, respectively the full and reduced differentiation matrices defined in §2, which are the discrete counterparts of the operators \mathcal{D} and $\bar{\mathcal{D}}$ respectively contained in \mathcal{A} and $\bar{\mathcal{A}}$. The puncturing of \mathbf{D}_N is implemented by removal of one row and one column (see [24, p.125]) to form the reduced matrix $\bar{\mathbf{D}}_N$.

equivalently, via (29),

$$u - u_N = (\bar{\mathcal{J}} - \bar{\mathcal{A}})^{-1} \bar{\mathcal{J}} (\mathcal{A} u_N - u_N + f), \quad (35)$$

which has the merit over (34) of avoiding the need to compute both the residual $\rho_N(x)$ and $\mathcal{A}_N u_N(x)$. Thus the error bound follows either from (34) in terms of the residual and operator-discretisation error as

$$\|u - u_N\| \leq \|(\bar{\mathcal{J}} - \bar{\mathcal{A}})^{-1}\| \|(\mathcal{A} - \mathcal{A}_N) u_N + \rho_N\|, \quad (36)$$

or from (35) in terms of only the numerical solution, and avoiding the need to compute $\mathcal{A}_N u_N$, as

$$\|u - u_N\| \leq \|(\bar{\mathcal{J}} - \bar{\mathcal{A}})^{-1}\| \|u_N - \mathcal{A} u_N - f\|. \quad (37)$$

Note that form (36) admits an asymptotic analysis (see §3.2) of the bound on the operator-discretisation term, whereas form (37) admits the interpretation that the error is proportional to the residual obtained when the numerical solution $u_N(x)$ of approximate IDE (29) is inserted into the exact IDE (23). Although the second term

$$\mathcal{S}_N \equiv \|u_N - \mathcal{A} u_N - f\| \quad (38)$$

in the product on the right-hand side of (37) can be computed directly using the numerical solution u_N , only a bound on the first such term can be obtained; this is now sought.

Because by (6), (14) and (30) the operators $\bar{\mathcal{A}}$ and $\bar{\mathcal{A}}_N$ are linear in their sub-operators, the procedure adopted in the IE error analysis in [12, §2.3] applied to \mathcal{K} and \mathcal{K}_N can here be extended to $\bar{\mathcal{A}}$ and $\bar{\mathcal{A}}_N$ in (34) without presenting the minutiae of the full derivation. Specifically, since both the numerical integration and differentiation schemes are convergent for all continuous functions on \mathcal{C} then, for sufficiently large N , by [4, Thm. 4.1.2], $(\bar{\mathcal{J}} - \bar{\mathcal{A}})^{-1}$ exists and is uniformly bounded, and

$$\|(\bar{\mathcal{J}} - \bar{\mathcal{A}})^{-1}\| \leq \mathcal{F}_N \equiv \frac{1 + \|(\bar{\mathcal{J}} - \bar{\mathcal{A}}_N)^{-1}\| \|\bar{\mathcal{A}}\|}{1 - \|(\bar{\mathcal{J}} - \bar{\mathcal{A}}_N)^{-1}\| \|(\bar{\mathcal{A}} - \bar{\mathcal{A}}_N) \bar{\mathcal{A}}\|}, \quad (39)$$

which defines the factor \mathcal{F}_N and in which the denominator is by construction positive. Then (37) yields a bound \mathcal{B}_N on the error norm \mathcal{E}_N given by

$$\mathcal{E}_N \equiv \|u - u_N\| \leq \mathcal{B}_N \equiv \mathcal{F}_N \mathcal{S}_N, \quad (40)$$

which both defines \mathcal{B}_N and expresses the Nyström IDE-approximation error in terms of only the numerical solution u_N . With \mathcal{S}_N given by (38), it therefore remains only to compute \mathcal{F}_N , to which end the element $\|(\bar{\mathcal{J}} - \bar{\mathcal{A}}_N)^{-1}\|$ in (39) is computed as $\|(\bar{\mathcal{J}} - \bar{\mathcal{A}}_N)^{-1}(\bar{\mathbf{1}})\|$ for the reasons given in [4, Eqns. (4.1.13)–(4.1.17)]. Accordingly, first define the function g_N by

$$g_N \equiv (\bar{\mathcal{J}} - \bar{\mathcal{A}}_N)^{-1}(\bar{\mathbf{1}}), \quad (41)$$

so that $g_N(x)$ is the solution of the IDE

$$g_N(x) - \bar{\mathcal{A}}_N g_N(x) = \bar{\mathbf{1}}. \quad (42)$$

Thus $g_N(x)$ satisfies the IDE

$$g_N(x) - \mathcal{A}_N g_N(x) = 1, \quad (43)$$

for which no BC is specified *a priori*. Imposing a BC and pursuing the argument yielding (32) would result in $g_N(x)$ satisfying

$$g_N(x) - \mathcal{A}_N g_N(x) = 1 - \sigma_N(x) \quad (44)$$

in which (*cf.* (28)) $\sigma_N(x) = \alpha_{k,N}(x)(g_N(\tilde{x}_{k,N}) - g_N^*(\tilde{x}_{k,N}))$ is the residual. Comparison of (43) and (44) therefore forces the residual to vanish for all $x \in [-1, 1]$, which requires $g_N(\tilde{x}_{k,N}) = g_N^*(\tilde{x}_{k,N})$, which is possible only if (43) is collocated at $x = \tilde{x}_{k,N}$. Therefore, by the argument following (27), collocation of (43) must occur at all nodes $\tilde{x}_{i,N}$, including $i = k$, thereby precluding the imposition of a BC. But since only a solution $g_N(x)$ of IDE (43) is required, such a collocation is sufficient, and hence the matrix system to be solved is

$$(\mathbf{I}_N - \mathbf{A}_N) \mathbf{g}_N = \mathbf{1} \quad (45)$$

in which \mathbf{I}_N and \mathbf{A}_N are as given in (20), and the vector entries of \mathbf{g}_N and $\mathbf{1}$ are given by

$$\{\mathbf{g}_N\}_i = g_N(\tilde{x}_{i,N}) \quad \text{and} \quad \{\mathbf{1}\}_i = 1. \quad (46)$$

Solving (45) yields the nodal solution whence $g_N(x)$ is given by the interpolation formula

$$g_N(x) = 1 + \sum_{j=1}^N \alpha_{j,N}(x) g_N(\tilde{x}_{j,N}), \quad (47)$$

using which the required inverse norm in (39) is computed as

$$\|(\bar{\mathcal{J}} - \bar{\mathcal{A}}_N)^{-1}\| = \|g_N\|. \quad (48)$$

The remaining components in (39) are computed using (again) the approach in [4, Eqns. (4.1.13)–(4.1.17)], which yields

$$\|\bar{\mathcal{A}}\| = \|\bar{\mathcal{A}}(1)\| = |\lambda| \|\bar{\mathcal{K}}(1)\| \quad (49)$$

and

$$\|(\bar{\mathcal{A}} - \bar{\mathcal{A}}_N) \bar{\mathcal{A}}\| = \|(\bar{\mathcal{A}} - \bar{\mathcal{A}}_N) \bar{\mathcal{A}}(1)\| = |\lambda| \|(\bar{\mathcal{A}} - \bar{\mathcal{A}}_N) \bar{\mathcal{K}}(1)\|. \quad (50)$$

As the analysis of §3.2 reveals [12, Eq. (20) *et seq.*], $\|(\bar{\mathcal{A}} - \bar{\mathcal{A}}_N) \bar{\mathcal{A}}\|$ will in general decay exponentially with N .

3.2. Asymptotic convergence rates for the error bound

Although (37) and (40) are used to compute the error bound \mathcal{B}_N , *a priori* estimates of the asymptotic convergence of the bound as $N \rightarrow \infty$ can be estimated using (36), which is algebraically equivalent to (37). The first term (the operator-discretisation error) in braces on the right-hand side of (36), δ_N say, is first bounded using (6), from which

$$\delta_N \equiv \|(\mathcal{A} - \mathcal{A}_N) u_N\| \leq \|\mu\| \|(\mathcal{D} - \mathcal{D}_N) u_N\| + |\lambda| \|(\mathcal{K} - \mathcal{K}_N) u_N\|, \quad (51)$$

	Legendre, $\nu = 0$	Radau, $\nu = 1$	Lobatto, $\nu = 2$	Asymptotic, $N \rightarrow \infty$
$\phi_N^{(\nu)}$	$\frac{2^{N-1} N(N+1)N!}{(2N)!}$	$\frac{2^N N^2 N!}{(2N)!}$	$\frac{2^N (2N-1)N!}{(2N)!}$	$\frac{2^{\nu-3/2}}{N^{(\nu^2-\nu-4)/2}} \left(\frac{e}{2N}\right)^N$
$\psi_N^{(\nu)}$	$\frac{2^{2N+1} (N!)^4}{(2N+1) \left((2N)!\right)^3}$	$\frac{2^{2N+2} (N!)^4}{\left((2N)!\right)^3}$	$\frac{2^{2N+2} (2N-1)^2 (N!)^4}{(N-1) \left((2N)!\right)^3}$	$\frac{2^{2\nu-1} \sqrt{\pi}}{N^{(1-2\nu)/2}} \left(\frac{e}{4N}\right)^{2N}$

Table 1: The coefficients $\phi_N^{(\nu)}$ and $\psi_N^{(\nu)}$ that respectively scale the numerical differentiation and quadrature error bounds in (52). The final column contains the respective asymptotic values as $N \rightarrow \infty$.

in which a combination of presently derived and standard results for Lagrange interpolation and Gaussian quadrature yields

$$\|(\mathcal{D} - \mathcal{D}_N) u_N\| \leq \phi_N^{(\nu)} \|u_N^{(N)}\| \quad \text{and} \quad \|(\mathcal{K} - \mathcal{K}_N) u_N\| \leq \psi_N^{(\nu)} \mathbb{K}_{2N-\nu}, \quad (52)$$

where the coefficients $\phi_N^{(\nu)}$ and $\psi_N^{(\nu)}$ for different node sets (i.e. different ν) are listed in Table 1, and

$$\mathbb{K}_M \equiv \max_{x, \tilde{x} \in [-1, 1]} \left| \frac{\partial^M}{\partial \tilde{x}^M} (K(x, \tilde{x}) u_N(\tilde{x})) \right|, \quad (53)$$

the argument on the right-hand side of which appears (with $M = 2N$) in the mean-value remainder of the N -point Gauss-Legendre-quadrature error $(\mathcal{K} - \mathcal{K}_N) u_N$. By (51), (52) and (53), the operator-discretisation error is bounded by

$$\delta_N \leq \phi_N^{(\nu)} \|\mu\| \|u_N^{(N)}\| + |\lambda| \psi_N^{(\nu)} \mathbb{K}_{2N-\nu}. \quad (54)$$

As $N \rightarrow \infty$ it is readily shown, using the asymptotic limits in the last column of Table 1, that

$$\frac{\psi_N^{(\nu)}}{\phi_N^{(\nu)}} \rightarrow \frac{2^{\nu+1/2} \sqrt{\pi}}{N^{(5-\nu-\nu^2)/2}} \left(\frac{e}{8N}\right)^N, \quad (55)$$

the right-hand side of which is, irrespective of ν , of the order of double-precision machine error for $N \approx 10$. That is, (55) reveals that, for practical purposes, in general (54) may be well approximated by

$$\delta_N \leq \phi_N^{(\nu)} \|\mu\| \|u_N^{(N)}\|, \quad N \gg 1. \quad (56)$$

Since it is readily determined from the entries in the last column of Table 1 that $\phi_N^{(\nu)} \sim O(N^{-N})$ and $\psi_N^{(\nu)} \sim O(N^{-2N})$ as $N \rightarrow \infty$, the predicted rate (56) of error convergence is valid when, via (54),

$$\|u_N^{(N)}\| \sim o(N^N) \quad \text{and} \quad \mathbb{K}_{2N-\nu} \sim o(N^{2N}), \quad N \rightarrow \infty; \quad (57)$$

that is, the conditions under which the present error analysis holds are non-restrictive and realisable in a plethora of situations. By contrast, it is worth noting that similar spectrally accurate *a priori* estimates

cannot emerge from the approach of [18], in which the Volterra component is integrated using Simpson's rule.

Though the asymptotic large- N behaviour of $\rho_N(x)$, which also appears on the right-hand side of (36), cannot be explicitly determined using (28), note that, since both $u_N(\tilde{x}_{k,N})$ and $u_N^*(\tilde{x}_{k,N})$ in (28) are given by a Nyström process for which (56) yields the error-convergence rate, the difference $u_N(\tilde{x}_{k,N}) - u_N^*(\tilde{x}_{k,N})$ in (28) must also be proportional to the same rate, i.e.,

$$\|\rho_N\| \sim \phi_N^{(\nu)} \|u_N^{(N)}\|, \quad N \rightarrow \infty, \quad (58)$$

and hence the entire second term on the right-hand side of (36) converges to zero at the rate in (56). Thus, via (36), (40), (56) and (58), and provided conditions (57) are met, the overall asymptotic error-convergence rate is

$$\mathcal{E}_N \equiv \|u - u_N\| \sim \phi_N^{(\nu)} \|u_N^{(N)}\|, \quad N \rightarrow \infty. \quad (59)$$

In §4, all predicted asymptotic rates (56), (58) and (59) are validated, on test problems, against the explicitly computed error bound given by (37).

Finally, by defining

$$\kappa(x) \equiv \int_{-1}^1 K(x, \tilde{x}) d\tilde{x} \quad \text{and} \quad \mathbb{L}_M \equiv \max_{x, \tilde{x} \in [-1, 1]} \left| \frac{\partial^M}{\partial \tilde{x}^M} (K(x, \tilde{x}) \kappa(\tilde{x})) \right|, \quad (60)$$

and employing the argument used to obtain (57), it is readily seen that, provided

$$\|\kappa^{(N)}\| \sim o(N^N) \quad \text{and} \quad \mathbb{L}_{2N-\nu} \sim o(N^{2N}), \quad N \rightarrow \infty, \quad (61)$$

then (50) and (a modified) (56) reveal that the denominator in (39) behaves as $1 + O(N^{-N})$ as $N \rightarrow \infty$, and hence the numerator of (39) is positive by construction, as demanded by the compact operator theory underlying the entire error analysis. As the results of §4 reveal, the asymptotic results derived above are in practice realised for relatively low values of N .

4. Test problems, results and discussion

Using the `Maple` algebraic manipulator, implementation of the theory of the preceding sections was conducted on all nodal distributions on two test problems: first, a method-validation problem with a known solution, and; second, a novel formulation of an Euler-Bernoulli beam-deflection problem, atypical in the sense that the (simply-supported) beam has a non-uniform cross-section, thereby inducing a spatially-dependent flexural rigidity that precludes the *a priori* determination of an exact solution.

4.1. Test-problem 1: validation using a known exact solution

In the specific case that the sub-components of (1) are

$$\begin{aligned} \mu(x) &= x^4 - 4, \quad K(x, \tilde{x}) = x^2 \tilde{x} \sin \tilde{x}, \quad \lambda = \frac{1}{2}, \quad u(-1) = 1 + \cos 1 \quad \text{and} \\ f(x) &= (3x^3 - 1)x^3 + (x^4 - 4) \sin x + \cos x + \frac{1}{8}(2 \cos 2 - \sin 2 - 96)x^2, \end{aligned} \quad (62)$$

the exact solution of (1) is $u(x) = \cos x - x^3$. Using this solution and the sub-components in (62), it is readily established that, as $N \rightarrow \infty$: (a) $\|u^{(N)}\| \sim 1$ and $\mathbb{K}_{2N} \sim 2^{2N}N$, and so the error-convergence criterion (57) is satisfied, and; (b) $\|\kappa^{(N)}\| = 0$ and $\mathbb{L}_{2N} \sim 16(\sin 1 - \cos 1)N^3$, and hence by (61) the theory of §3 valid. Accordingly, it is expected that the new method will predict accurate error estimates. In the terminology of [13], (62) is deemed to be a “smooth” problem: both computed and predicted errors for more challenging so-called “Runge”, “steep” and “oscillatory” problems [13, Table 1 and Figure 5] are less accurate than those for the “smooth” problem. However, since such kernels are implemented and comprehensively analysed in [13], they are not pursued herein.

For test problem (62), BCs were enforced both directly (see §4.3) and indirectly (see §4.3), and the choice of these alternatives was examined. In all numerical experiments, only the Lobatto nodal distribution, for which $\nu = 2$, was used; this includes both end-points and in theory [12, Table 1], though not always in practice, yields the largest error bound of all distributions introduced immediately after (7).

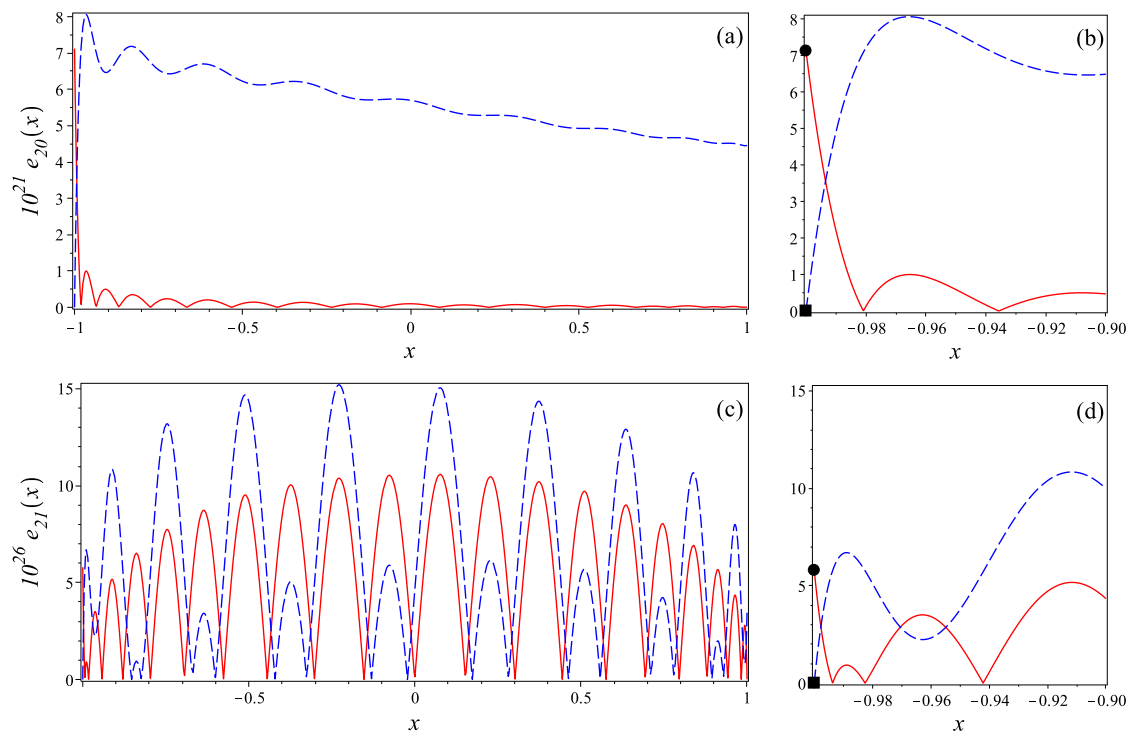


Figure 1: Effect of BC implementation on numerical error of problem (62). Plots show case-1 (solid lines, red online) and case-2 (dashed lines, blue online) absolute errors $e_N(x) \equiv |u(x) - u_N(x)|$ using Lobatto nodes with (a,b) $N = 20$ and (c,d) $N = 21$, for which error profiles are qualitatively similar to those for other values of N even and N odd respectively. Disparate vertical scalings in (a,b) and (c,d) indicate spectral decay of e_N with N . In expanded plots (b) and (d) of the “BC-zones” in (a) and (c) respectively, black circles on solid lines show a non-zero error at the BC location $\xi = -1$, confirming prediction (A.7) that case-1 interpolation fails to recover the true BC; black squares on dashed lines confirm prediction (A.12) that case-2 interpolation recovers the exact BC. The case-2 results are for $k = 1$ in interpolation formula (A.11); the effect of varying k is considered in Figure 2.

Figure 1 demonstrates the effect on the absolute-error distribution in $[-1, 1]$ of implementing the BC as

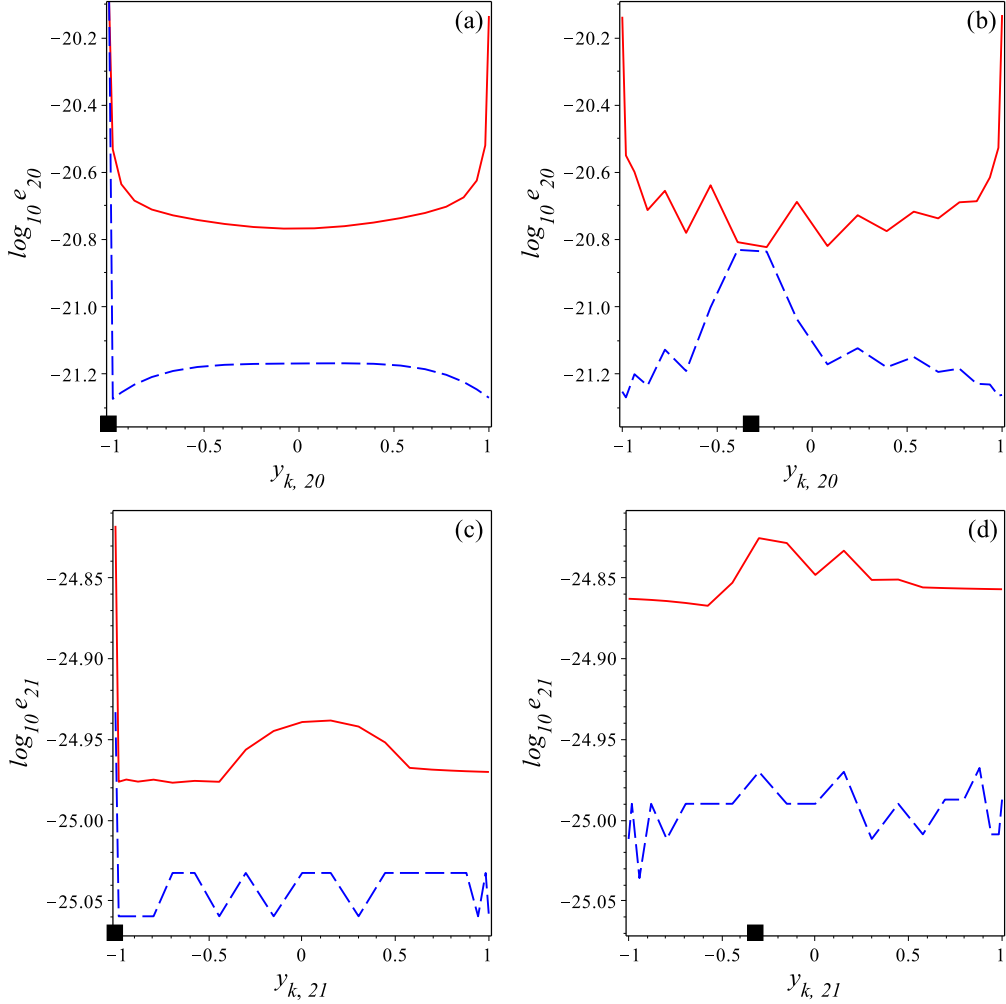


Figure 2: Effect of varying k in case-2 BC interpolation (A.11) for problem (62). Logarithmic plots show error norms $\|e_N\|_\infty$ (solid lines, red online) and, purely for comparison, $\|e_N\|_2$ (dashed lines, blue online) using Lobatto nodes with (a,b) $N = 20$ and (c,d) $N = 21$ and BC applied at (a,c) $\xi = -1$ and (b,d) $\xi = -1/\pi$; BC locations are annotated by black squares. Curves link nodal data generated by varying k from 1 to N in (A.11). Comparison (see vertical scales) of (a) with (c) and (b) with (d) reveals that the disparity between the maximum and minimum values of $\|e_N\|_\infty$ is a spectrally decreasing functions of N .

either case 1 or case 2 in problem (62). BC abscissa $\xi = -1$ was chosen so that a Lobatto grid would admit a direct comparison between case 1 and case 2, the latter using $k = 1$. Results confirm predictions (A.7) and (A.12) regarding which case recovers the true BC in the final Nyström interpolation (A.11). Note in Figures 1(a,b) the Runge phenomenon in the case-1 error in the region nearest to the BC abscissa.

Figure 2 demonstrates the effect of varying $1 \leq k \leq N$, the arbitrary node number assigned in (A.8), on both the infinity- and 2-norms of the absolute error. BC abscissae $\xi = -1$ and $\xi = -1/\pi$ were used in experiments, the latter irrational number enforcing a case-2 BC implementation. For N even/odd, the norms were minimised/maximised for values of k near to $N/2$, though the absolute variation with k is a spectrally decreasing function of N and is due to rounding errors in the inversion of (A.10). Corresponding

results for other BCs, e.g. at $\xi = 1$ and $\xi = 1/\pi$, show similar behaviour.

Figure 3 depicts clear evidence of spectrally accurate agreement between the actual computational error norm \mathcal{E}_N defined in (40) and the new theoretical bound \mathcal{B}_N computed in terms of only the numerical solution u_N using (38)–(40). This level of agreement moreover validates the argument used to obtain the function $g_N(x)$ via (45)–(47). Note that, as required, the bound exceeds the error, though experiments revealed that this was not necessarily the case if $\|(\bar{\mathcal{J}} - \bar{\mathcal{A}}_N)^{-1}\|$ in (39) was computed other than as $\|(\bar{\mathcal{J}} - \bar{\mathcal{A}}_N)^{-1}(\bar{\mathbf{I}})\|$ [4, Eqns. (4.1.13)–(4.1.17)].

Case-2 BC results in Figure 3 were computed using $k = 1$ in (A.11): in experiments in which k was varied, minor perturbations in the displayed results were observed (as expected from the results in Figure 2), though perturbed errors and bounds either increased or decreased together so that the bound always exceeded the error. Computations performed on the Legendre and Radau nodal distributions, for which $\nu = 0$ and $\nu = 1$ respectively, showed only minor quantitative perturbations from those discussed. Further, more detailed, observations on test problem (62) are discussed in the caption of Figure 3.

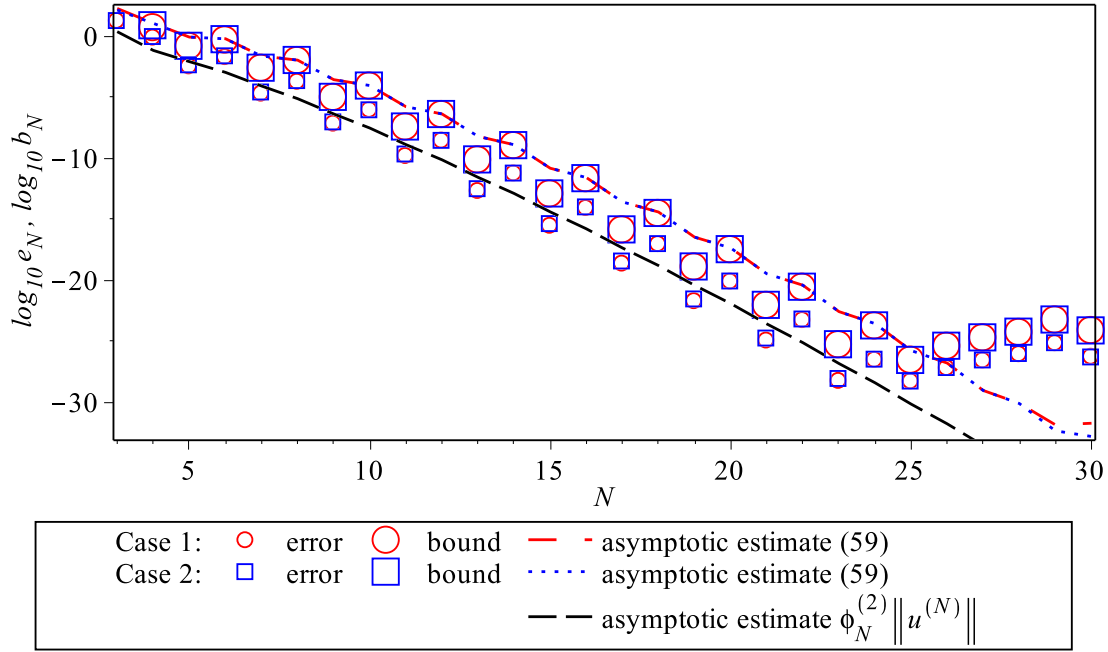


Figure 3: Logarithmic plot of the actual computational error \mathcal{E}_N for test problem (62) (small symbols, here annotated as e_N) and predicted bound \mathcal{B}_N in (40) (large symbols, here annotated as b_N), solved using Lobatto nodes with BC at $\xi = -1$. Circles (red online) and squares (blue online) respectively denote results of case 1 and case 2, the latter with $k = 1$ in (A.11). The agreement between \mathcal{E}_N and \mathcal{B}_N is impressive, and the prediction \mathcal{B}_N captures well the rate of convergence to zero. The undulating (coincident on this scale) dashed lines show the predicted asymptotic error-convergence rate (59), and the smooth dashed line shows the same rate but with $\|u_N^{(N)}\|$ replaced by $\|u^{(N)}\|$. The undulation in, and greater magnitude of, the former rates results from the ill-conditioning [6] of the N -fold discrete differentiation of the inversion formula (12). Indeed, the undulation with the parity of N is even more pronounced in the numerical results themselves.

4.2. Test-problem 2: Euler-Bernoulli beam-deflection problem with varying flexural rigidity

Having validated the error-prediction approach in §4.1, consider now the problem of determining the deflection $w(x)$ under loading $q(x)$ of a static, horizontal, prismatic beam spanning the (scaled) interval $x \in [-1, 1]$ at whose ends BCs are enforced. When the cross-sectional area of the beam is uniform, the solution of the fourth-order ubiquitous Euler-Bernoulli differential equation satisfied by $w(x)$ is straightforward, and explicit solutions $w(x)$ for various BCs abound in a plethora of sources.

When, however, the cross-sectional area of the beam is a function of x , so is the resulting second moment of area $I(x)$ and, therefore, also the flexural rigidity, i.e. the product of $I(x)$ and the elastic modulus $E(x)$ of the beam. In this case, the Euler-Bernoulli BVP demands numerical solution.

To fix a specific problem, consider the case of a circular cylindrical beam of radius $R(x)$ with simply-supported beam ends, so that the BCs are $w(-1) = w(1) = w'(-1) = w'(1) = 0$. Additionally, both the elastic modulus and loading will be taken as constant along the beam, i.e. $E(X) = E$ and $Q(X) = Q_0$ in (B.1): note that these assumptions are not restrictions *per se*.

Transformation of the resulting fourth-order, two-point BVP is algebraically complex but readily achieved using an algebraic manipulator. A novel (to the authors' knowledge) derivation of the scaling and transformation is, for reasons of clarity, deferred to Appendix B, in which appears the next equation, repeated here to facilitate discussion. It can be shown (see (B.23)) that the beam deflection $w(x)$ satisfies a first-order Fredholm IDE of the form

$$w'(x) - \sigma_a(x)w'(-1) - \sigma_b(x)w'(1) + A(x)w(x) - \int_{-1}^1 W(x, \tilde{x})w(\tilde{x}) = \Phi(x), \quad (63)$$

in which $A(x)$ is given by (B.3), the source function $\Phi(x)$ (which incorporates the beam loading) by (B.24) and the coefficient and kernel functions $\sigma_a(x)$, $\sigma_b(x)$, and $W(x, \tilde{x})$ by (B.28)–(B.30). First note that, unlike problem (62), the kernel $W(x, \tilde{x})$ in (63) has, by (B.30), a finite discontinuity along the line $x = \tilde{x}$ that is expected, upon replacing K by W in (53), to erode the accuracy of the error bounds; this expectation is borne out in the results in §4. Second, (63) contains not the expected (see (1)) single BC $w(-1)$ but rather two BCs $w'(\pm 1)$ that were not given *a priori*: this is a direct result of the specified BCs occurring in two pairs, one each at second and zeroth order. However, this is readily accommodated at the implementation stage because, when (63) is discretised on nodes $\{x_1, \dots, x_N\}$, the unknown $w'(\pm 1)$ can be eliminated using the zeroth-order BCs $w_1 = 0$ and $w_N = 0$ in (8) as

$$w'(-1) \approx w'_1 = \sum_{j=1}^N D_{1j}w_j \quad \text{and} \quad w'(1) \approx w'_N = \sum_{j=1}^N D_{Nj}w_j. \quad (64)$$

Since here $E(x) = E$, a constant, the function $A(x)$ defined in (B.3) reduces to

$$A(x) = \frac{2I'(x)}{I(x)}. \quad (65)$$

Assume that variations, e.g. due to manufacturing defects, in $R(x)$ relative to a mean value R_0 along the

cylindrical beam length are small in comparison to the radius, i.e.

$$R(x) = R_0(1 + \epsilon\tau(x)) \quad (66)$$

where, since the scaled beam length is 2, we require $|\epsilon| \ll R_0 \ll 2$ and $\|\tau\| = O(1)$ on $[-1, 1]$. Using as a datum the second moment of area of such a cylindrical beam,

$$I_0 = \frac{1}{4}\pi R_0^4, \quad (67)$$

the second moment corresponding to (66) is

$$I(x) = I_0(1 + \epsilon\tau(x))^4. \quad (68)$$

In the present example the test perturbation

$$\tau(x) = x(1 + x^2) \quad (69)$$

is used whence, via (65)–(69), the “Euler-Bernoulli IDE” (63) has no exact solution since the integral term in the source function $\Phi(x)$ cannot be determined analytically for a general loading $q(x)$. However, for the constant loading $Q(X) = Q_0$, equations (68), (69), (B.3) and (B.37) yield

$$q(x) = \frac{q_0}{(1 + \epsilon x + \epsilon x^3)^4}, \quad (70)$$

so that, because $|\epsilon| \ll 2$, an approximate theoretical solution $\tilde{w}(x; \epsilon)$ of (63) can be sought as a series expansion in ϵ , resulting in, to second order,

$$\begin{aligned} \tilde{w}(x; \epsilon) \sim & \frac{q_0}{504}(x-1)(x+1)(21(x^2-5) - 24x(x^2-2)(x^2+3)\epsilon \\ & + (28x^8 + 73x^6 - 11x^4 - 221x^2 - 221)\epsilon^2), \quad \epsilon \rightarrow 0. \end{aligned} \quad (71)$$

The derivation of (71), which offers a rudimentary means of checking approximate numerical solutions of (63), is omitted since it is mechanical and readily automated using an algebraic manipulator.

A comparison of numerical solutions of the Euler-Bernoulli problem (63) and the asymptotic series solution (71) is portrayed in Figure 4, which confirms excellent agreement, to visual accuracy, between the numerical and asymptotic solutions. A more detailed consideration of errors, along with predicted bounds, is depicted in Figure (5) in which, in the absence of an exact solution of (63), errors are computed relative to a “converged” numerical solution computed with $N = 90$ Lobatto nodes.

Although broadly following the error trends observed in Figure 3 for test problem (62), Figure 5 confirms relatively larger errors and deceleration of their convergence to zero in (63), which is due to a combination of the discontinuity along $x = \tilde{x}$ of the kernel $W(x, \tilde{x})$ defined in (B.30) and the unavoidable approximation of $w'(\pm 1)$ in (63) using the numerical differentiation in (64). An additional concomitant effect of this treatment of $w'(\pm 1)$ is that the bounds (but not the errors) in Figure 5 are barely dependent⁵ on ϵ ,

⁵Closer inspection reveals marginally greater bounds for $\epsilon = 0.1$ than for $\epsilon = 0.01$.

because approximation (64) removes the terms involving $\sigma_a(x)$ and $\sigma_b(x)$ from the amended error theory. Nonetheless, the errors and predicted bounds for the Euler-Bernoulli test problem (63) are of a magnitude comparable to those of the “steep” and “oscillatory” test problems considered in [13, Figure 5(c,d)].

Finally, note that, for this problem, the inversion formula (based on (12) and (63)) for $w_N(x)$ utilises the discontinuous kernel (B.30), thereby introducing a saw-tooth behaviour in $w_N(x)$ between the nodes. This is presently averted by replacing the inversion formula with Lagrange interpolation through the N Legendre-nodal values, so that the resulting $(N - 1)^{\text{st}}$ -order polynomial has a vanishing N^{th} derivative: thus, an asymptotic error-convergence estimate (59) cannot be derived.

4.3. Limitations of the Theory

Problems (62) and (63) respectively have smooth and finitely-discontinuous kernels: as the results depicted in Figures 3 and 5 show, the new IDE error-prediction method works well in both cases and particularly so in the former. However, in the presence of more challenging kernels, this may not be so. Typical examples are: (a) $K(x, \tilde{x}) = e^{-\omega(x-\tilde{x})^2}$ ($\omega \in \mathbb{R}^+$), representing an isolated peak along the diagonal; such kernels arise in the consideration of non-local Eringen stress models (see, e.g., [11, 1, 17, 14, 25, 26]) in solid mechanics; (b) $K(x, \tilde{x}) = \tilde{x}^2/(1 + 25x^2)$, for which the solution is plagued by the Runge phenomenon; (c) $K(x, \tilde{x}) = x^2 e^{20\tilde{x}}$, which kernel is locally “steep”, and; (d) $K(x, \tilde{x}) = x^2 \cos 20\tilde{x}$, which is “highly oscillatory”. Though the actual computation errors converge with increasing N for all of the challenging-kernel problems, the bound theory does not do so for problems (a) and (c), though for different reasons. In (a), the failure occurs at the level of implementation because, when evaluating

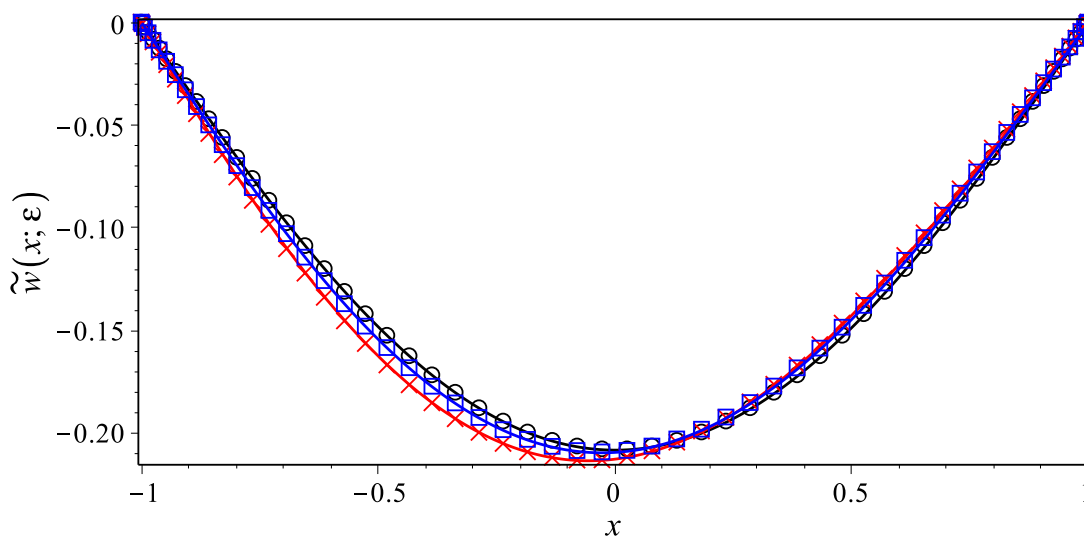


Figure 4: Cylindrical-beam profiles computed using $N = 60$ Lobatto nodes in the discretisation of approximate IDE (63) for a “beam-radius-defect” function given by (66) and (69). Nodal values for $\epsilon = 0, 0.05$ and 0.1 are respectively shown as circles (black online), squares (blue online) and crosses (red online), and the smooth curves joining them are the second-order series approximation $\tilde{w}(x; \epsilon)$ given by (71) with $q_0 = -1$ in (70); note that $\tilde{w}(x; 0)$ recovers the well-known supported-uniform-beam solution (B.38).

$\bar{\mathcal{A}} \bar{\mathcal{K}}(1)$ in (50), it is generally not possible to perform the double integration as a closed-form function of x , as required in the denominator of the bound (39). In (c), the bound predictions become negative because the denominator in (39) is negative: that is, condition [4, Eq. (4.1.22)], required for (39) to hold, is violated. Although in (a) it is possible to bound the uncomputable term in (50) by a modified (54), this also yields negative error predictions as the second condition in (61) is violated. In (b), although the error bound is computable because $\|(\bar{\mathcal{A}} - \bar{\mathcal{A}}_N)\bar{\mathcal{A}}\|$ can be computed exactly (cf. comment immediately below (50)), the kernel yields a value of $\kappa(x)$ as

$$\kappa(x) = \frac{2}{3(1+25x^2)} \Rightarrow \|\kappa^{(N)}\| = O(N^N), \quad (72)$$

which violates the first condition in (61).

In conclusion, a novel and readily implementable approach has been presented for the *a priori* computation of error bounds inherent in the application of general Nyström methods for approximating the solutions of one-dimensional Fredholm IDEs. Bounds are computed explicitly, to spectral accuracy, and in terms of only the available numerical solution. The method has been exemplified on a novel practical problem in Euler-Bernoulli beam-deflection theory, and it is hoped that this flexible and widely applicable approach will serve as a useful tool for future research on other applications of the ubiquitous IDE (1).

References

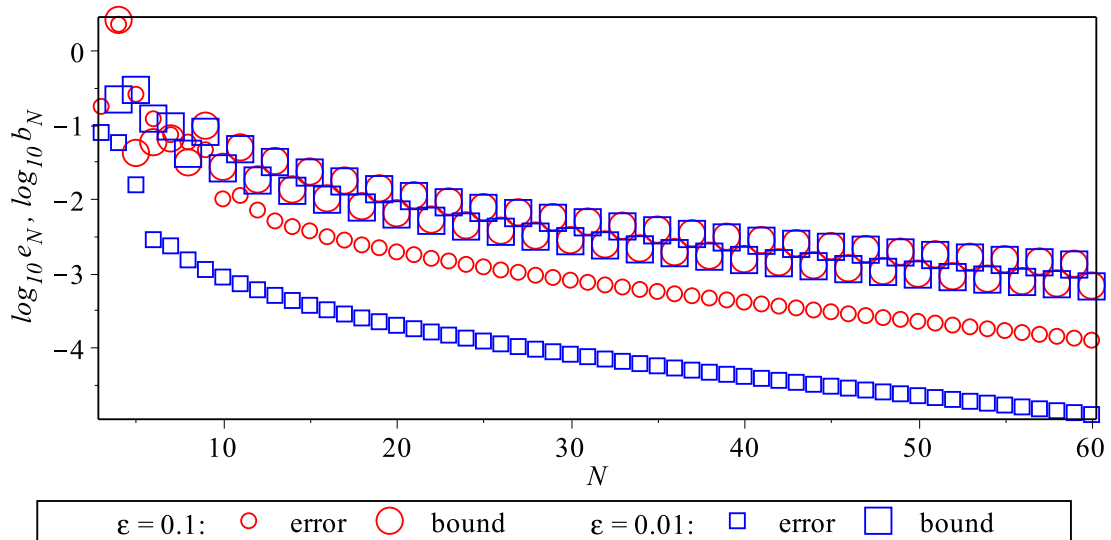


Figure 5: Logarithmic plot of case-1 errors \mathcal{E}_N (e_N on axis, denoted by small symbols) and predicted error bounds \mathcal{B}_N (b_N on axis, denoted by large symbols) for Euler-Bernoulli test problem (63). In the absence of an exact solution, errors are computed relative to a numerical solution obtained with $N = 90$ nodes. Circles (red online) and squares (blue online) correspond to results computed using $\epsilon = 0.1$ and $\epsilon = 0.01$ respectively. The agreement between \mathcal{E}_N and \mathcal{B}_N is less impressive than those in Figure 3; see text for an explanation of this phenomenon.

- [1] R. ABDOLLAHI AND B. BOROOMAND, *Nonlocal elasticity defined by Eringen's integral model: Introduction of a boundary layer method*, Int. J. Solids Struct., 51 (2014), 1758–1780.
- [2] O. A. ARQUB, M. AL-SMADI AND N. SHAWAGFEH, *Solving Fredholm integro-differential equations using reproducing kernel Hilbert space method*, Appl. Math. Comput., 219 (2013), 8938–8948.
- [3] E. ARUCHUNAN AND J. SULAIMAN, *Quarter-sweep Gauss-Seidel method for solving first order linear Fredholm integro-differential equations*, Matematika, 27 (2011), 199–208.
- [4] K. E. ATKINSON, *The Numerical Solution of Integral Equations of the Second Kind*, Cambridge University Press, Cambridge, UK, 1997.
- [5] N. BILDIK, A. KONURALP AND S. YALÇINBAŞ, *Comparison of Legendre polynomial approximation and variational iteration method for the solutions of general linear Fredholm integro-differential equations*, Comput. Math. Appl., 59 (2010), 1909–1917.
- [6] K.S. BREUER AND R.M. EVERSON, *On the Errors Incurred Calculating Derivatives Using Chebyshev Polynomials*, J. Comput. Phys., 99 (1992), 56–67.
- [7] P. DARANIA AND A. EBADIAN, *A method for the numerical solution of the integro-differential equations*, Appl. Math. Comput., 188 (2007), 657–668.
- [8] T.A. DRISCOLL AND N. HALE, *Rectangular spectral collocation*, IMA J. Numer. Anal., 36 (2016), 108–132.
- [9] G.N. ELNAGAR, *Optimal Control Computation For Integro-Differential Aerodynamic Equations*, Math. Meth. Appl. Sci., 21 (1998), 653–664.
- [10] G.N. ELNAGAR AND A. KHAMAYSEH, *Numerical Solution of Non-stationary Aero-autoelasticity Integro-differential Operator Equations*, Math. Meth. Appl. Sci., 22 (1999), 501–513.
- [11] E. EMMRICH AND O. WECKNER *Analysis and numerical approximation of an integro-differential equation modeling non-local effects in linear elasticity*, Mathematics and Mechanics of Solids, 12 (2007), 363–384.
- [12] A. I. FAIRBAIRN AND M. A. KELMANSON, *Spectrally accurate Nyström-solver error bounds for 1-D Fredholm integral equations of the second kind*, Appl. Math. Comput., 315 (2017), 211–223.
- [13] A. I. FAIRBAIRN AND M. A. KELMANSON, *Error analysis of a spectrally accurate Volterra-transformation method for solving 1-D Fredholm integro-differential equations*, Int. J. Mech. Sci., 144 (2018), 382–391.
- [14] J. FERNÁNDEZ-SÁEZA, R. ZAERA, J.A. LOYA AND J.N. REDDY, *Bending of Euler-Bernoulli beams using Eringen's integral formulation: A paradox resolved*, Int. J. Eng. Sci, 99 (2016), 107–116.
- [15] S. M. HOSSEINI AND S. SHAHMORAD, *Tau numerical solution of Fredholm integro-differential equations with arbitrary polynomial bases*, Appl. Math. Model., 27 (2003), 145–154.
- [16] Z. JACKIEWICZ, M. RAHMAN AND B. WELFERT, *Numerical solution of a Fredholm integro-differential equation modelling neural networks*, Appl. Numer. Math., 56 (2006), 423–432.

- [17] P. KHODABAKHSHI AND J.N. REDDY, *A unified integro-differential nonlocal model*, Int. J. Eng. Sci., 95 (2015), 60–75.
- [18] P. LINZ, *A method for the approximate solution of linear integro-differential equations*, SIAM J. Numer. Anal., 11 (1974), 137–144.
- [19] K. MALEKNEJAD AND M. ATTARY, *An efficient numerical approximation for the linear class of Fredholm integro-differential equations based on Cattani’s method*, Commun. Nonlinear Sci. Numer. Simulat., 16 (2011), 2672–2679.
- [20] M. PERELMUTER, *Integral-Differential Equations for Stress Analysis at the Bridged Zone of Interface Cracks*, in C. Constanda and P.J. Harris (Eds.), *Integral Methods in Science and Engineering*, Birkhäuser, Boston, (2010), 287–298.
- [21] M. PERELMUTER, *Bridged crack model of interfacial toughness*, Structural Integrity Procedia, 2 (2016), 2030–2037.
- [22] P. K. SAHU AND S. RAY, *Legendre spectral collocation method for Fredholm integro-differential equation with variable coefficients and mixed conditions*, Appl. Math. Comput., 268 (2015), 575–580.
- [23] S.A. SILLING AND E. ASKARI, *A meshfree method based on the peridynamic model of solid mechanics*, Computers and Structures, 83 (2005), 1526–1535.
- [24] L. N. TREFETHEN, *Spectral Methods in MATLAB*, SIAM, Philadelphia, 2000.
- [25] M. TUNA AND M. KIRCA, *Exact solution of Eringen’s nonlocal integral model for bending of Euler-Bernoulli and Timoshenko beams*, Int. J. Eng. Sci., 105 (2016) 80–92.
- [26] Y.B. WANG, X.W. ZHU AND H.H. DAI, *Exact solutions for the static bending of Euler-Bernoulli beams using Eringen’s two-phase local/nonlocal model*, AIP Advances, 6 (2016) 085114.
- [27] S. YALÇINBAŞ AND M. SEZER, *The approximate solution of high-order linear volterra-fredholm integro-differential equations in terms of taylor polynomials*, Appl. Math. Comput., 112 (2000), 291–308.
- [28] S. YALÇINBAŞ, M. SEZER AND H. H. SORKUN, *Legendre polynomial solutions of high-order linear Fredholm integro-differential equations*, Appl. Math. Comput., 210 (2009), 334–349.

Appendix A. Implementation of BCs

To clarify description of the BC implementation, it is useful to amend the notation in (17) to

$$\mathcal{A}_N u_N^*(x) \equiv \sum_{j=1}^N \alpha_{j,N}(x) u_N^*(\tilde{x}_{j,N}), \quad (\text{A.1})$$

in which the notation $u_N^*(\tilde{x}_{j,N})$ indicates a nodal value of $u_N(x)$ determined by collocation in the first stage of the Nyström process, rather than by interpolation in the second stage. Hence there are two cases to consider, depending on whether collocation or interpolation is used to implement the BC.

Case 1: direct enforcement of the BC through collocation

This case requires the BC abscissa ξ to coincide with a node⁶, i.e. $\xi = y_{k,N}$ for some $1 \leq k \leq N$. Renaming u_N as \tilde{u}_N in this case, BC (2) is incorporated directly as

$$\tilde{u}_N^*(y_{k,N}) \leftarrow \tilde{\zeta} \equiv \zeta, \quad (\text{A.2})$$

which notation is to be interpreted as assignment of $\tilde{\zeta}$, whose value has been set equal to ζ , to the single nodal value $\tilde{u}_N^*(y_{k,N})$ for the purposes of collocation. Assigning the k^{th} nodal value as per (A.2) and omitting the now-redundant collocation at $x = y_{k,N}$, (18) becomes

$$\sum_{\substack{j=1 \\ j \neq k}}^N (\delta_{ij} - \alpha_{j,N}(\tilde{x}_{i,N})) \tilde{u}_N^*(\tilde{x}_{j,N}) = f(\tilde{x}_{i,N}) + \tilde{\zeta} \alpha_{k,N}(\tilde{x}_{i,N}), \quad i = 1(1)N, i \neq k, \quad (\text{A.3})$$

so that the reduced $(N-1) \times (N-1)$ system is given by

$$(\tilde{\mathbf{I}}_N - \tilde{\mathbf{A}}_N) \tilde{\mathbf{u}}_N^* = \tilde{\mathbf{f}}_N, \quad (\text{A.4})$$

in which tilded quantities follow by removing the k^{th} rows (and, for the matrices, k^{th} columns) of their counterparts in (19), and by augmenting the right-hand side of (19) in accordance with that of (A.3). Solution of (A.4) yields the $(N-1)$ components $\tilde{u}_N^*(\tilde{x}_{j,N})$ of the nodal solution vector $\tilde{\mathbf{u}}_N^*$ which, when augmented with (A.2), give the Nyström interpolation formula (cf. (16))

$$\tilde{u}_N(x) = f(x) + \tilde{\zeta} \alpha_{k,N}(x) + \sum_{\substack{j=1 \\ j \neq k}}^N \alpha_{j,N}(x) \tilde{u}_N^*(\tilde{x}_{j,N}), \quad x \in [-1, 1]. \quad (\text{A.5})$$

Setting $x = \tilde{x}_{i,N}$ with $i \neq k$, comparison of (A.3) and the right-hand side of (A.5) gives the latter equal to $\tilde{u}_N^*(\tilde{x}_{i,N})$, i.e. $\tilde{u}_N(\tilde{x}_{i,N}) = \tilde{u}_N^*(\tilde{x}_{i,N})$ for $i \neq k$. However, when $i = k$ – equivalently, $x = \tilde{x}_{k,N}$ – the right-hand side of (A.5) cannot be deduced from (A.3) and so, in general, and by (A.2),

$$\tilde{u}_N(\tilde{x}_{k,N}) \neq \tilde{u}_N^*(\tilde{x}_{k,N}) \leftarrow \tilde{\zeta}. \quad (\text{A.6})$$

Equivalently, since $\tilde{x}_{k,N} = \xi$, (A.6) gives

$$\tilde{u}_N(\xi) \neq \tilde{\zeta} = \zeta; \quad (\text{A.7})$$

that is, despite direct assignment (A.2) of the BC at the collocation stage, it is not recovered exactly as per (2) at the interpolation stage (A.5). A numerical demonstration of the non-recovery of the BC in case 1 is given in §4.

⁶ This can happen when, e.g., $\xi = \pm 1$ is chosen for the BC location and any of Lobatto, Left-Radau or Right-Radau quadrature are used, all of which contain abscissae with $|\tilde{x}_{j,N}| = 1$.

Case 2: indirect enforcement of the BC through interpolation

This implementation works for any BC location, whether or not it coincides with a node. Renaming u_N as \widehat{u}_N in this case, an arbitrary value of $1 \leq k \leq N$ is chosen; substituting (2) into (16) and eliminating the nodal value $\widehat{u}_N^*(y_{k,N})$ yields the pseudo-BC (cf. (A.2)) nodal assignment

$$\widehat{u}_N^*(y_{k,N}) \leftarrow \widehat{\zeta} \equiv \frac{1}{\alpha_{k,N}(\xi)} \left(\zeta - f(\xi) - \sum_{\substack{j=1 \\ j \neq k}}^N \alpha_{j,N}(\xi) \widehat{u}_N^*(\tilde{x}_{j,N}) \right), \quad (\text{A.8})$$

in which it is noted that, for arbitrary k, ξ, N, ν and $K(x, \tilde{x})$, the value of $\alpha_{k,N}(\xi)$ computed using (15) will be non-zero with probability arbitrarily close to one. Substitution of (A.8) into (18) gives, after some manipulation, the $(N-1) \times (N-1)$ system

$$\begin{aligned} \sum_{\substack{j=1 \\ j \neq k}}^N \left(\delta_{ij} - \alpha_{j,N}(\tilde{x}_{i,N}) + \frac{\alpha_{k,N}(\tilde{x}_{i,N})}{\alpha_{k,N}(\xi)} \alpha_{j,N}(\xi) \right) \widehat{u}_N^*(\tilde{x}_{j,N}) \\ = f(\tilde{x}_{i,N}) + \frac{\alpha_{k,N}(\tilde{x}_{i,N})}{\alpha_{k,N}(\xi)} (\zeta - f(\xi)), \quad i = 1(1)N, i \neq k. \end{aligned} \quad (\text{A.9})$$

In (reduced) matrix format, this is (cf. (A.4))

$$(\widehat{\mathbf{I}}_N - \widehat{\mathbf{A}}_N) \widehat{\mathbf{u}}_N^* = \widehat{\mathbf{f}}_N, \quad (\text{A.10})$$

in which $\widehat{\mathbf{I}}_N = \widetilde{\mathbf{I}}_N$, $\widehat{\mathbf{u}}_N^* = \widetilde{\mathbf{u}}_N^*$, and the elements of $\widehat{\mathbf{A}}_N$ and $\widehat{\mathbf{f}}_N$ are readily computed from the information in (A.9). Solution of (A.10) yields the $(N-1)$ components $\widehat{u}_N^*(\tilde{x}_{j,N})$ of the nodal solution vector $\widehat{\mathbf{u}}_N^*$. Then (A.8) gives $\widehat{u}_N^*(y_{k,N})$, i.e. $\widehat{\zeta}$, using which the Nyström interpolation formula is (cf. (16))

$$\widehat{u}_N(x) = f(x) + \widehat{\zeta} \alpha_{k,N}(x) + \sum_{\substack{j=1 \\ j \neq k}}^N \alpha_{j,N}(x) \widehat{u}_N^*(\tilde{x}_{j,N}), \quad x \in [-1, 1]. \quad (\text{A.11})$$

In this case, setting $x = \xi$ in (A.11) and then eliminating the resulting term $\widehat{\zeta} \alpha_{k,N}(\xi)$ on the right-hand side using pseudo-BC (A.8) gives (cf. (A.7))

$$\widehat{u}_N(\xi) = \zeta; \quad (\text{A.12})$$

that is, in case 2, the Nyström interpolation (A.11) recovers the exact BC (2). Additionally, by an argument analogous to the one following (A.5), the omission of $x = \tilde{x}_{k,N}$ from the collocation (A.9) means that (A.11) yields (cf. (A.6))

$$\widehat{u}_N(\tilde{x}_{k,N}) \neq \widehat{u}_N^*(\tilde{x}_{k,N}) \leftarrow \widehat{\zeta}. \quad (\text{A.13})$$

Appendix B. Transformation of Euler-Bernoulli beam equation into IDE (1)

Appendix B.1. Variable flexural rigidity

Consider the ubiquitous fourth-order two-point BVP comprising the Euler-Bernoulli static-beam equation for the deflection $W(X)$ of a loaded beam of undeformed length L ,

$$(EIW''')' = Q, \quad X \in [0, L], \quad (\text{B.1})$$

in which a prime denotes differentiation with respect to X , $I(X)$ is the second moment of area about the centroid of the beam's cross-section, $Q(X)$ is the distributed load per unit length and $E(X)$ is the elastic modulus of the beam, which in the numerical experiments in §4.2 is taken as the constant Young's modulus of mild steel, $E \approx 2 \times 10^{11}$ Pa. Additionally, (B.1) is augmented by four boundary conditions (BCs), at $X = 0$ and $X = L$, on $W(X)$ and/or its derivatives. In the general case that the flexural rigidity $F(X) \equiv E(X)I(X)$ of the beam is a varying function of X , the deflection is non-dimensionalised using $W(X) = Lw(X)$ then (B.1) is scaled from the interval $[0, L]$ onto $[-1, 1]$ using $X = \frac{1}{2}L(1 + x)$ and rewritten as the second-order differential equation in canonical form

$$w''''(x) + A(x)w'''(x) + B(x)w''(x) = q(x), \quad x \in [-1, 1], \quad (\text{B.2})$$

in which

$$A(x) = \frac{2F'(x)}{F(x)}, \quad B(x) = \frac{F''(x)}{F(x)} \quad \text{and} \quad q(x) = \frac{L^3Q(x)}{16F(x)}, \quad (\text{B.3})$$

wherein now all primes now refer to differentiation with respect to x . Subsequent analysis is facilitated by defining $C(x)$ as

$$C(x) \equiv A'(x) - B(x), \quad (\text{B.4})$$

whence direct integration of (B.2) using

$$w'''(x) = w'''(-1) + \int_{-1}^x w''''(\tilde{x}) d\tilde{x} \quad (\text{B.5})$$

yields, after employing triple and double integration by parts on respectively the second and third terms in (B.2), the third-order Volterra IDE for $w(x)$,

$$w'''(x) = \int_{-1}^x K_3(x, \tilde{x}) w(\tilde{x}) d\tilde{x} + \lambda_3(x) + \mu_3(x), \quad (\text{B.6})$$

in which

$$K_3(x, \tilde{x}) = C''(\tilde{x}), \quad (\text{B.7})$$

$$\lambda_3(x) = C'(-1)w(-1) - C(-1)w'(-1) + A(-1)w''(-1) + w'''(-1), \quad (\text{B.8})$$

$$\mu_3(x) = \int_{-1}^x q(\tilde{x}) d\tilde{x} - C'(x)w(x) + C(x)w'(x) - A(x)w''(x). \quad (\text{B.9})$$

Integration of (B.6)–(B.9) using

$$w''(x) = w''(-1) + \int_{-1}^x w'''(s) ds, \quad (\text{B.10})$$

requires reversed-variable double integration of the integrand of $K_3(x, \tilde{x})$, which yields

$$\int_{-1}^x \int_{-1}^s C''(\tilde{x}) w(\tilde{x}) d\tilde{x} ds = \int_{-1}^x \int_{\tilde{x}}^x C''(\tilde{x}) w(\tilde{x}) ds d\tilde{x} = \int_{-1}^x (x - \tilde{x}) C''(\tilde{x}) w(\tilde{x}) d\tilde{x}; \quad (\text{B.11})$$

this, along with repeated integration by parts of $\mu_3(x)$, leads to the second-order Volterra IDE for $w(x)$,

$$w''(x) = \int_{-1}^x K_2(x, \tilde{x}) w(\tilde{x}) d\tilde{x} + \lambda_2(x) + \mu_2(x), \quad (\text{B.12})$$

in which

$$K_2(x, \tilde{x}) = (x - \tilde{x}) C''(\tilde{x}) - A''(\tilde{x}) - 2C'(\tilde{x}), \quad (\text{B.13})$$

$$\lambda_2(x) = (1 + x) \lambda_3(x) - (A'(-1) + C(-1)) w(-1) + A(-1) w'(-1) + w''(-1), \quad (\text{B.14})$$

$$\mu_2(x) = \int_{-1}^x (x - \tilde{x}) q(\tilde{x}) d\tilde{x} + (A'(x) + C(x)) w(x) - A(x) w'(x). \quad (\text{B.15})$$

Proceeding similarly,

$$w'(x) = w'(-1) + \int_{-1}^x w''(s) ds \quad (\text{B.16})$$

now yields the first-order Volterra IDE for $w(x)$,

$$w'(x) = \int_{-1}^x K_1(x, \tilde{x}) w(\tilde{x}) d\tilde{x} + \lambda_1(x) + \mu_1(x), \quad (\text{B.17})$$

in which

$$K_1(x, \tilde{x}) = \frac{1}{2}(x - \tilde{x})^2 C''(\tilde{x}) - (x - \tilde{x})(A''(\tilde{x}) + 2C'(\tilde{x})) + 2A'(\tilde{x}) + C(\tilde{x}), \quad (\text{B.18})$$

$$\lambda_1(x) = -\frac{1}{2}(1 + x)^2 \lambda_3(x) + (1 + x) \lambda_2(x) + A(-1) w(-1) + w'(-1), \quad (\text{B.19})$$

$$\mu_1(x) = \frac{1}{2} \int_{-1}^x (x - \tilde{x})^2 q(\tilde{x}) d\tilde{x} - A(x) w(x). \quad (\text{B.20})$$

Further progress is specific to the imposed BCs: for illustrative purposes, simply-supported beam ends are assumed, whence

$$w(-1) = \alpha, \quad w(1) = \beta \quad \text{and} \quad w''(-1) = w''(1) = 0, \quad (\text{B.21})$$

for some real, possibly non-zero, constants α and β . The unknown $w'''(-1)$ enters $w'''(x)$ in (B.6) through $\lambda_3(x)$, and hence by (B.14) and (B.12) it enters $w''(x)$, and by (B.19) and (B.17) it enters $w'(x)$. Setting $x = 1$ in both (B.6) and (B.12) and employing the BCs $w''(-1) = w''(1) = 0$ generates two equations for determining $w'''(-1)$ and $w'''(1)$, only the former of which is required to proceed: there results

$$\begin{aligned} w'''(-1) = \frac{1}{2} \left\{ \int_{-1}^1 (A''(\tilde{x}) + 2C'(\tilde{x}) - (1 - \tilde{x}) C''(\tilde{x})) w(\tilde{x}) d\tilde{x} - \int_{-1}^1 (1 - \tilde{x}) q(\tilde{x}) d\tilde{x} \right. \\ \left. + (A'(-1) + C(-1) - 2C'(-1)) \alpha - (A'(1) + C(1)) \beta \right. \\ \left. + (2C(-1) - A(-1)) w'(-1) + A(1) w'(1) \right\}, \quad (\text{B.22}) \end{aligned}$$

in which $w'(-1)$ and $w'(1)$ are still unknown. After splitting the integral in (B.22) at $\tilde{x} = x$, back-substitution into (B.8), (B.14), (B.19) and (B.17) yields a first-order Fredholm IDE for $w(x)$ in the form

$$w'(x) - \sigma_a(x) w'(-1) - \sigma_b(x) w'(1) + A(x) w(x) - \int_{-1}^1 W(x, \tilde{x}) w(\tilde{x}) = \Phi(x), \quad (\text{B.23})$$

in which the source term is given by

$$\Phi(x) = \sigma_\alpha(x) \alpha + \sigma_\beta(x) \beta + \int_{-1}^1 Q(x, \tilde{x}) q(\tilde{x}) d\tilde{x}, \quad (\text{B.24})$$

wherein

$$\sigma_\alpha(x) = A(-1) - \frac{1}{4}(1+x)(3-x)(A'(-1) + C(-1)), \quad (\text{B.25})$$

$$\sigma_\beta(x) = -\frac{1}{4}(1+x)^2(A'(1) + C(1)), \quad (\text{B.26})$$

$$Q(x, \tilde{x}) = \begin{cases} \frac{1}{4}(1+\tilde{x})(x^2 - 2(x-\tilde{x}) - 1) & \tilde{x} \in (-1, x) \\ \frac{1}{4}(\tilde{x}-1)(1+x)^2 & \tilde{x} \in (x, 1) \end{cases}. \quad (\text{B.27})$$

The remaining, as-yet-undefined, terms in (B.23) are

$$\sigma_a(x) = 1 + \frac{1}{4}(1+x)(3-x)A(-1), \quad (\text{B.28})$$

$$\sigma_b(x) = \frac{1}{4}(1+x)^2A(1), \quad (\text{B.29})$$

$$W(x, \tilde{x}) = \begin{cases} 2A'(\tilde{x}) + C(\tilde{x}) + \frac{1}{4}(1+\tilde{x})(x^2 - 2(x-\tilde{x}) - 1)C''(\tilde{x}) \\ \quad + (\tilde{x} + \frac{1}{4}(1-x)^2)(A''(\tilde{x}) + 2C'(\tilde{x})) & \tilde{x} \in (-1, x) \\ \frac{1}{4}(1+x)^2(A''(\tilde{x}) + 2C'(\tilde{x}) - (1-\tilde{x})C''(\tilde{x})) & \tilde{x} \in (x, 1) \end{cases}. \quad (\text{B.30})$$

Finally, division of equations (B.23) and (B.24) by $A(x)$ completes the transformation of the original fourth-order Euler-Bernoulli two-point BVP into a first-order Fredholm IDE of the second kind of the form (1) provided $A(x) \neq 0$ for $x \in [-1, 1]$. Although it is possible in principle to use IDE (B.23) to eliminate $w'(1)$ in terms of an integral over $[-1, 1]$ and then to determine $w(x)$ by further integration, the resulting expressions are so cumbersome and unwieldy that, for a general non-uniform-cross-sectional beam under general loading $q(x)$ in the Euler-Bernoulli equation (B.2), numerical integration of the kernel functions will invariably be required and so the extra algebraic step constitutes a Pyrrhic victory, particularly when noting that all of the analysis following (B.21) is BC-specific.

Appendix B.2. Constant flexural rigidity

A natural segue of the above offers a method for rapid recovery and extension of standard beam-deflection formulae which can be used to gauge numerical results when variations in flexural rigidity lead to only a perturbation of the main deflection. When the flexural rigidity $F(x)$ of the beam is constant, (B.3) and (B.4) yield $A(x) = B(x) = C(x) = 0$ and also

$$q(x) = \frac{L^3 Q(x)}{16EI_0}, \quad (\text{B.31})$$

in which I_0 is the easily calculated constant second moment of area of the uniform cross-section of the prismatic beam. Then (B.17)–(B.20) degenerate to

$$\begin{aligned} w'(x) = w'(-1) &+ \frac{1}{4} \int_{-1}^x (1+\tilde{x})(x^2 - 2(x-\tilde{x}) - 1) q(\tilde{x}) d\tilde{x} \\ &- \frac{1}{4} \int_x^1 (1+x)^2(1-\tilde{x}) q(\tilde{x}) d\tilde{x}, \end{aligned} \quad (\text{B.32})$$

integration of which demands not only (B.11) but also the additional variable-reversal rule

$$\int_{-1}^x \int_s^1 f(\tilde{x}) d\tilde{x} ds = \int_{-1}^x \int_{-1}^{\tilde{x}} f(\tilde{x}) ds d\tilde{x} + \int_x^1 \int_{-1}^x f(\tilde{x}) ds d\tilde{x} \quad (\text{B.33})$$

$$= \int_{-1}^x (\tilde{x} + 1) f(\tilde{x}) d\tilde{x} + \int_x^1 (x + 1) f(\tilde{x}) d\tilde{x}, \quad (\text{B.34})$$

for all suitably integrable functions $f(x)$ on $[-1, 1]$. This yields $w(x)$ in terms of $w'(-1)$, which can now be eliminated using the BC $w(1) = \beta$: the omitted cumbersome algebra is readily automated using an algebraic manipulator.

Accordingly, the non-dimensionalised deflection $w_s(x)$ of a simply-supported beam can be succinctly represented explicitly in terms of the (scaled) distributed load $q(x)$ per unit length as

$$w_s(x) = \alpha + \frac{1}{2}(\beta - \alpha)(x + 1) + \int_{-1}^1 Q_s(x, \tilde{x}) q(\tilde{x}) d\tilde{x}, \quad (\text{B.35})$$

in which

$$Q_s(x, \tilde{x}) = \begin{cases} \frac{1}{12}(x-1)(1+\tilde{x})(x^2 + \tilde{x}^2 + 2(\tilde{x} - x - 1)) & \tilde{x} \in (-1, x) \\ \frac{1}{12}(\tilde{x}-1)(1+x)(\tilde{x}^2 + x^2 + 2(x - \tilde{x} - 1)) & \tilde{x} \in (x, 1) \end{cases}. \quad (\text{B.36})$$

Formula (B.35) readily admits direct computation of simply-supported beam profiles for general load distributions $q(x)$ because all BCs are included *a priori* by construction. This appendix concludes with some common examples, in all of which both α and β are taken as zero in (B.35): viewed alternatively, the deflection computed is that from the straight line joining $(-1, \alpha)$ to $(1, \beta)$.

Define the parameter q_0 by

$$q_0 \equiv \frac{L^3 Q_0}{16EI_0}, \quad (\text{B.37})$$

where Q_0 is a constant (negative in the case of loading in the direction of gravity) and I_0 is defined in (67). When in (B.35) and (B.31) $q(x) = q_0$, one may readily obtain the non-dimensional deflection

$$w_s^{(c)}(x) = \frac{1}{24}q_0(x-1)(x+1)(x^2 - 5) \quad (\text{B.38})$$

and, for the loading $q(x) = \frac{1}{2}(x+1)q_0$ in (B.35) that changes linearly from zero at $x = -1$ to q_0 at $x = 1$, there immediately follows

$$W_s^{(\ell)}(x) = \frac{1}{720}q_0(x-1)(x+1)(x+3)(3x^2 + 6x - 25). \quad (\text{B.39})$$

Finally, a point load of magnitude q_0 at $x = c \in (-1, 1)$ is accommodated using the Dirac-delta loading $q(x) = q_0 \delta(x - c)$ in (B.35) to obtain

$$W_s^{(p)}(x) = \frac{1}{12}q_0 \left\{ (1+x)(1-c)(x^2 + c^2 + 2(x-c-1)) - 2(x-c)^3 H(x-c) \right\}, \quad (\text{B.40})$$

in which $H(x)$ is the Heaviside function. All of (B.38)–(B.40) can be rescaled onto $[0, L]$ using $x = 2X/L - 1$ to recover results in more familiar notation. Additionally, it is possible to accommodate other scenarios, e.g. cantilever-beam deformation, simply by changing the BCs at stage (B.21).